

# Effect of Annealing Temperature of Gold Doped Reduced Graphene Oxide Counter Electrode on the Performance of Dye-sensitized Solar Cell

M.Y.A. Rahman\*, A.S. Sulaiman, A.A. Umar

Institute of Microengineering and Nanoelectronics (IMEN), Universiti Kebangsaan Malaysia, 43600, Bangi, Selangor, Malaysia

\*E-mail: [mohd.yusri@ukm.edu.my](mailto:mohd.yusri@ukm.edu.my)

Received: 15 January 2018 / Accepted: 5 March 2018 / Published: 10 May 2018

---

This paper is concerned with the use of gold doped reduced graphene oxide (rGO) films, replacing costly platinum films as a counter electrode in dye-sensitized solar cell (DSSC). The influence of annealing treatment of the electrode on the performance parameters of the device has been investigated. The XRD analysis reveals that crystallite size of GO increases with annealing temperature. The 140 °C sample possesses the highest transmission in visible region. The DSSC utilizing the sample annealed at 120 °C performed the highest  $\eta$  of 0.134%, respectively due to the longest carrier lifetime.

---

**Keywords:** annealing treatment, counter electrode, dye-sensitized solar cell, gold, graphene oxide

## 1. INTRODUCTION

Counter electrode in DSSC serves as a medium to receive electrons from external circuit resulted in by photovoltaic effect to reduce oxidizing species to reducing species such as reducing triiodide to iodide and polysulfide to sulfide. Platinum films have widely been used as counter electrode in DSSC since it is electrochemically stable against the redox couple of iodide/triiodide and polysulfide/sulfide in liquid electrolyte. Nevertheless, the main drawback of platinum is that it is very expensive material as counter electrode in DSSC. Carbon film has been utilized as counter electrode in DSSC as an alternative to costly platinum since it has high electronic conductivity, corrosion resistance, electrochemical reactivity and low cost [1-3].

Graphene can also be utilized as counter electrode in the device due to its unique properties such as good electrical property and high electrochemical stability [4-10]. It was found that the efficiency of the DSSC utilizing graphene films counter electrode was comparable with that using

platinum films counter electrode [4-10]. In our previous work, we have utilized reduced graphene oxide (rGO) as counter electrode in DSSC and achieved an efficiency of 0.09% [11]. The effect of GO content on the performance of the device has been investigated.

The efficiency was improved by doping RGO with metallic material such as gold. The doping of rGO with metal has been carried out by Soo and his group who doped silver into rGO films for use as a catalyst in fuel cell [12]. Xue and his co-workers used nitrogen doped graphene films as counter electrode in DSSC [13]. Nitrogen doped graphene films were utilized as superior counter electrode for DSSC [14]. Phosphorous doped reduced graphene oxide (rGO) was employed as counter electrode in DSSC [15].

In this work, we have doped rGO with gold in order to improve the electronic conductivity of RGO films. Gold doped reduced graphene oxide (rGO) films were then utilized as a counter electrode in DSSC. The originality of this work is the utilization of gold doped rGO films as counter electrode of DSSC. The goal of this work is to investigate the effect of annealing temperature of gold doped rGO on the performance parameters of the DSSC.

## 2. EXPERIMENTAL

### 2.1 Preparation of gold doped rGO and characterizations

0.1 g GO powders were dissolved in 50 ml deionized water and the solution was sonicated for 1 h. 2 mg gold (III) chloride trihydrate ( $\text{HAuCl}_4 \cdot 3\text{H}_2\text{O}$ ) powder which is equivalent to 2 wt.% was then added into the solution and sonicated for 30 minutes. The solution was stirred for 5 minutes. The solution was finally spin coated 3 times on ITO substrate at 1000 rpm for 15 s to get sufficient thickness of gold doped RGO on the substrate. The sample was annealed at 100 °C in argon atmosphere for 15 minutes. These procedures were repeated by annealing the samples at 110, 120, 130 and 140 °C, respectively. The structure of the samples was analyzed by XRD technique. The optical transmission of the samples was characterized by UV-Vis spectrophotometer. The bonding analysis was performed by Raman spectrometer. The Raman spectra have been obtained under 532 nm excitation wavelength of incident laser beam.

### 2.2 Fabrication and performance study of DSSC

The DSSC was fabricated by using  $\text{TiO}_2$  films as photoanode. The  $\text{TiO}_2$  films were prepared on ITO substrate via liquid phase deposition technique at 40 °C. 0.5 M  $\text{LiI}$ /0.05 M  $\text{I}_2$ /0.5 M TBP in acetonitrile containing iodide/triiodide redox couple was used as a liquid electrolyte. Gold doped RGO films annealed at various temperatures were utilized as counter electrode. A parafilm was sandwiched between the  $\text{TiO}_2$  film and gold doped RGO film counter electrode. A structure containing  $\text{TiO}_2$  film and gold doped RGO film was clamped in order to optimize the interfacial contact of these device components. The electrolyte was injected into the structure via a capillary. The current-voltage curves in dark and under illumination of 100  $\text{mW cm}^{-2}$  tungsten light were recorded by a Keithley high-

voltage source model 237 interfaced with a personal computer. The illuminated area of the device was  $0.23 \text{ cm}^2$ . The electrochemical impedance spectroscopy (EIS) technique was also employed to determine the bulk resistance ( $R_b$ ), charge interfacial resistance ( $R_{ct}$ ) and charge carrier lifetime at the applied voltage of 0.4 V.

### 3. RESULTS AND DISCUSSION

Fig. 1 shows the XRD spectra for the samples annealed at various temperatures. It is noticed that there are quite a lot of noises in the spectra. It is observed that there is only one dominant peak which is located at  $10.5^\circ$  corresponding with the miller index (002), belonging to rGO. The peaks of aurum are not observed in the spectra, signifying that aurum atom has successfully been doped into the lattice of RGO. It is also found that the peak intensity at this diffraction angle increases with annealing temperature up to  $130^\circ\text{C}$  and then drops. The crystallite size of the samples is illustrated in Table 1. The table shows the increasing trend of crystallite size with annealing temperature except  $130^\circ\text{C}$  samples. This agrees well with the literature that crystallite size increases with temperature.

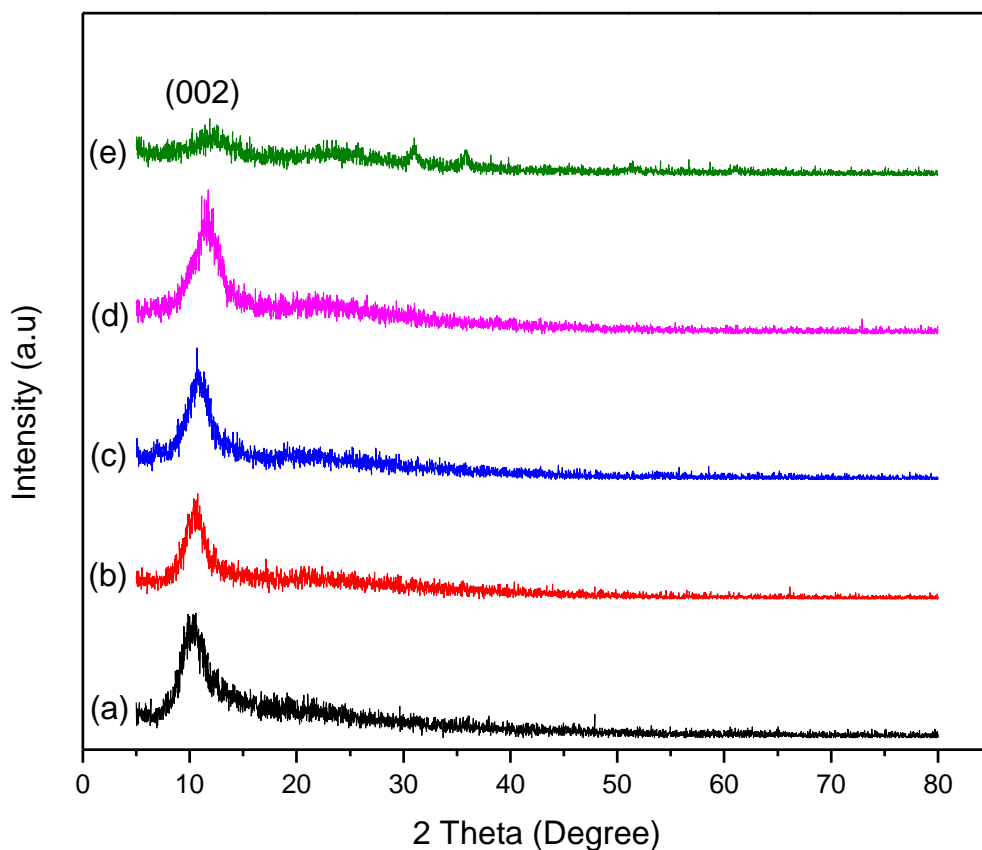


**Figure 1.** XRD spectra for Au doped RGO samples annealed at (a) 100, (b) 110, (c) 120, (d) 130 and (e)  $140^\circ\text{C}$

**Table 1.** Full width half maximum (FWHM) and crystallite of the samples with various annealing temperatures

Temperature (°C)	FWHM	Crystallite Size (Å)
100	2.045	42.7
110	1.540	51.2
120	1.340	61.0
130	1.593	47.3
140	1.409	73.8

Fig. 2 depicts the UV-Vis transmission spectra of gold doped rGO film sample with various annealing temperatures. It is noticed from the spectra that the transmission area varies with the annealing temperature. The 120 °C sample shows the smallest area of light transmission followed by 130, 100, 110 and 140 °C samples. The 140 °C sample shows one transmission peak in UV region which is in the region 300-400 nm and another one peak in visible region which is in the region 400-700 nm. It is found that the transmission in visible region is higher than that in UV region. It is also found that the transmission in IR region with the wavelength above 700 nm is higher than that in UV and visible region for all samples.

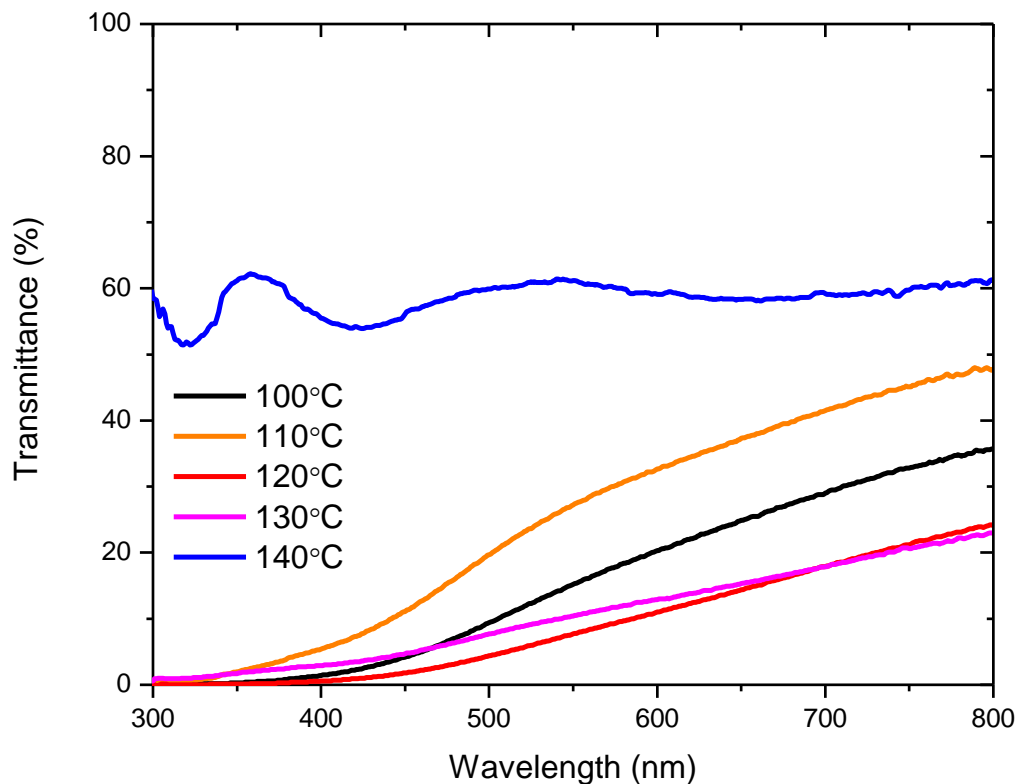
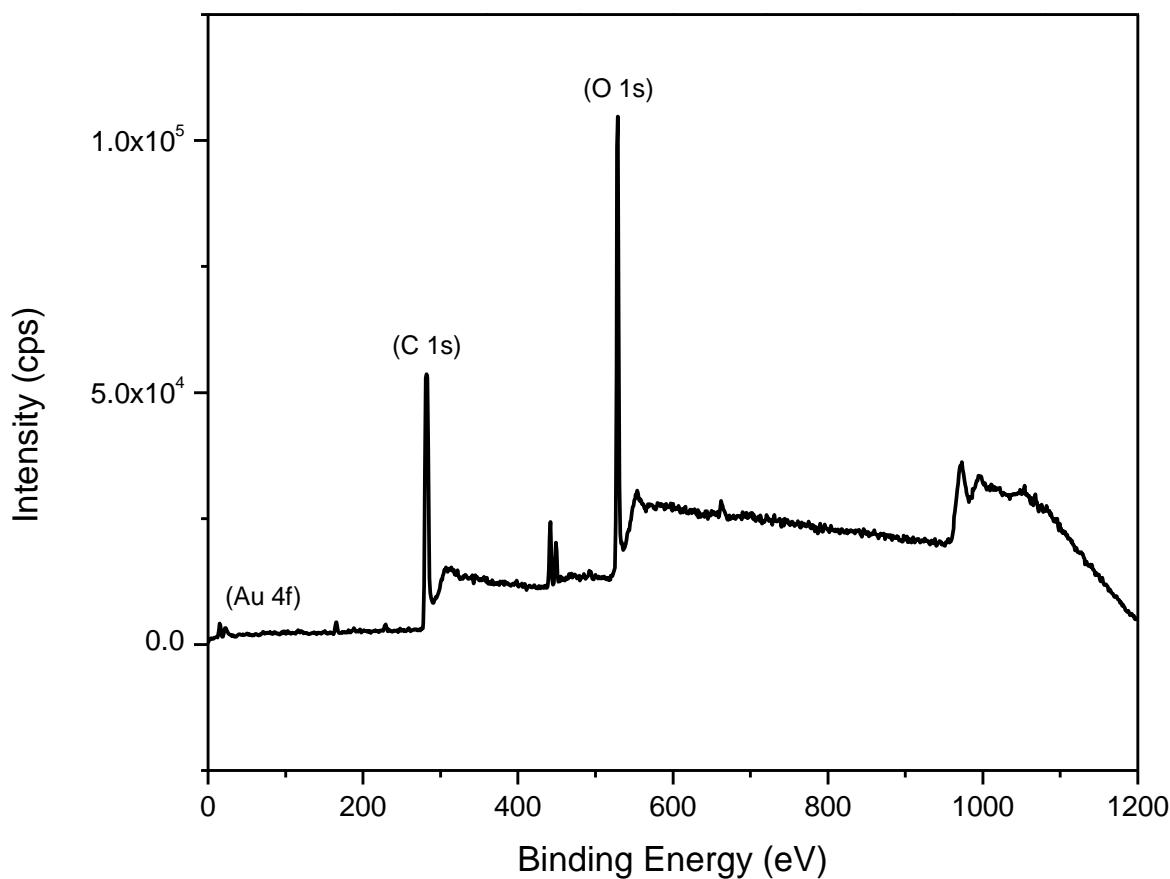
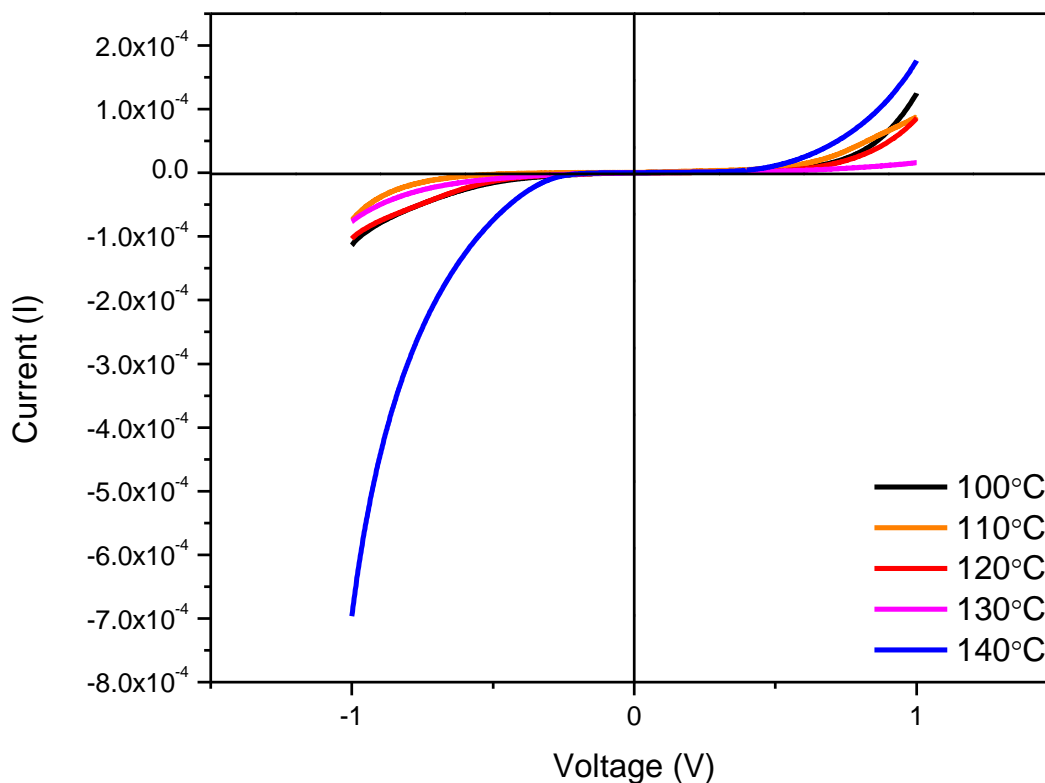
**Figure 2.** UV-Vis transmission spectra of gold doped rGO film sample with various annealing temperatures

Fig. 3 shows the XPS spectrum for the Au-doped rGO which was annealed at 120 °C. The spectrum shows that the peak of Au 4f, C 1s and O 1s is at the binding energy of 81.3, 295.8 and 537.9 eV, respectively. The presence of short peak of Au indicates that its atoms are incorporated into RGO. The short peak of Au is due to its small amount doped into RGO that is only 2 wt.%. The large amounts of oxygen functional groups such as C-O bonds, carbonyls or carboxylates on GO are removed during the annealing treatment at 120 °C [15].



**Figure 3.** XPS spectrum for the sample annealed at 120 °C

Fig. 4 shows the *I-V* curves in dark of the DSSCs utilizing gold doped RGO films counter electrodes with various annealing temperatures. It is noticeable that the devices do not show rectification property since the dark current in reverse bias also called leak current is larger than that in forward bias. In other words, the leak current curves are unsymmetrical with the forward current curves. The difference in the leak current is quite significant signifying that the annealing temperature gold influences the leak current. However, the difference in forward current is small, indicating that the temperature does not affect the forward bias dark current. The device with the sample prepared at 110 °C, gold possesses the lowest leak current followed by the devices utilizing the samples annealed at 130, 120, 100 and 140 °C.

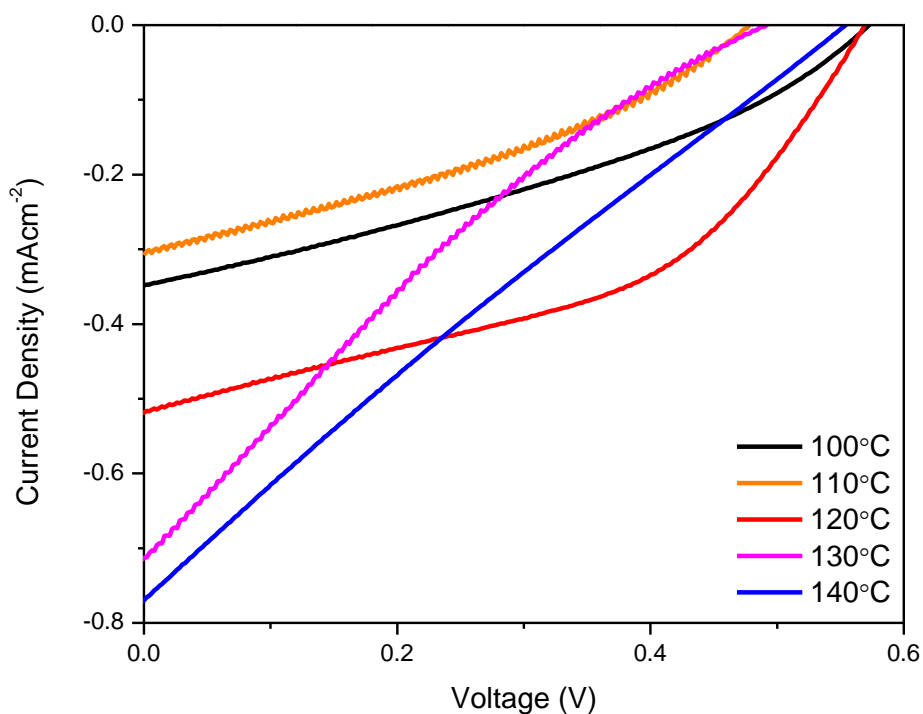


**Figure 4.** *I-V* curves of the devices in dark with various annealing temperatures of gold doped rGO

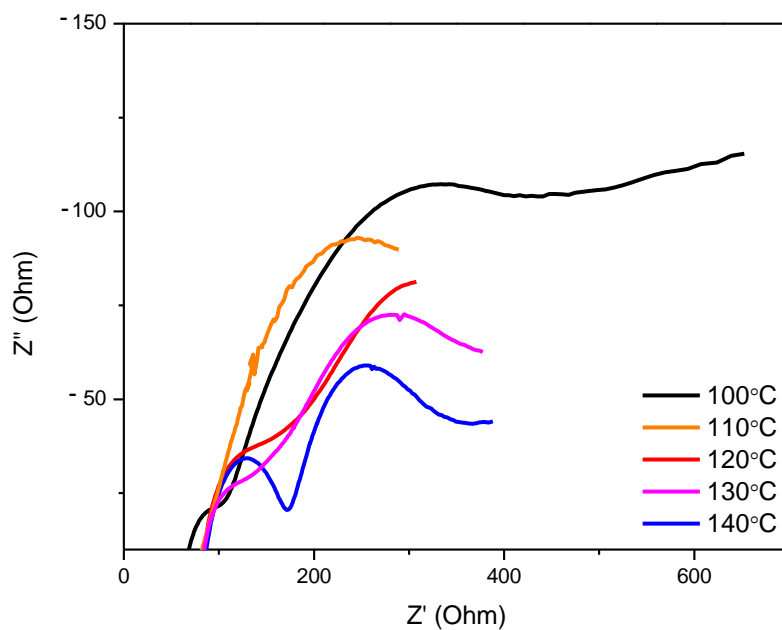
Fig. 5 shows the current density-voltage (*J-V*) curves of the DSSC utilizing the samples annealed at various temperatures at  $100 \text{ mW cm}^{-2}$  light illuminations. The device annealed at  $110 \text{ }^\circ\text{C}$  generates the lowest output power, followed by 100, 130, 140 and  $120 \text{ }^\circ\text{C}$  samples. The curve of 130 and  $140 \text{ }^\circ\text{C}$  devices have high slope indicating high internal resistance of the devices. The curve of  $140 \text{ }^\circ\text{C}$  devices is represented by linear line, similar to the one reported by Rahman et al. 2005 [16]. However, the shape of the curve of  $130 \text{ }^\circ\text{C}$  device is the same as that was reported by Choi et al. 2011 [17]. Rahman et al. 2016 also reported the same shape of the *J-V* curve obtained from the DSSC utilizing pure rGO counter electrode [11]. The photovoltaic parameters are extracted from Fig. 5 and illustrated in Table 2.

Fig. 6 shows Nyquist plots of the DSSC utilizing gold doped rGO films counter electrode annealed at various temperatures. From the plots, two semicircles are observed, namely, smaller semicircle representing bulk resistance ( $R_b$ ) of the device and bigger semicircle denoting charge transfer resistance ( $R_{ct}$ ). Both resistances are computed from the real impedance ( $Z'$ ). The imaginary impedance ( $Z''$ ) is negative since it is not used to determine both resistances. The bulk resistance is attributed by the resistance of each component of the device. The charge transfer resistance is contributed by the resistance at the interface of  $\text{TiO}_2\text{-N719/electrolyte}$  and  $\text{electrolyte/gold doped RGO}$ . Both resistances are estimated from the plots and presented in Table 2. From the table, it is found that  $R_b$  is smaller than  $R_{ct}$ . The device utilizing the counter electrode prepared at  $110 \text{ }^\circ\text{C}$  possesses the lowest  $R_b$  followed by the devices with 130, 100, 120 and  $140 \text{ }^\circ\text{C}$  samples. The device

with the temperature of 140 °C has the lowest  $R_{ct}$ , followed by the devices utilizing 110, 130, 100 and 120 °C samples.



**Figure 5.** *J-V* curves of the devices with various annealing temperatures of gold doped rGO under illumination of  $100 \text{ mW cm}^{-2}$



**Figure 6.** Nyquist plots of the DSSCs with various annealing temperatures of gold doped RGO

Fig. 7 illustrates the Bode plots of the devices utilizing gold doped rGO film counter electrode with various annealing temperatures. It is found that there is one peak appears in each plot, representing resonant frequency of each device. The carrier lifetime was computed from the frequency and presented in Table 2. Carrier lifetime is defined as the period taken by the charge carrier which is electron to travel across the interface of  $\text{TiO}_2$ -N719 dye before recombining with hole at the interface of electrolyte/gold doped rGO. According to the table, the device utilizing the sample annealed at  $100^\circ\text{C}$  possesses the shortest lifetime, followed the devices utilizing  $140$ ,  $130$  and  $120^\circ\text{C}$  samples. However, the carrier lifetime of  $110^\circ\text{C}$  sample cannot be computed since its resonant frequency is not observed in the bode plot shown in Fig. 7.

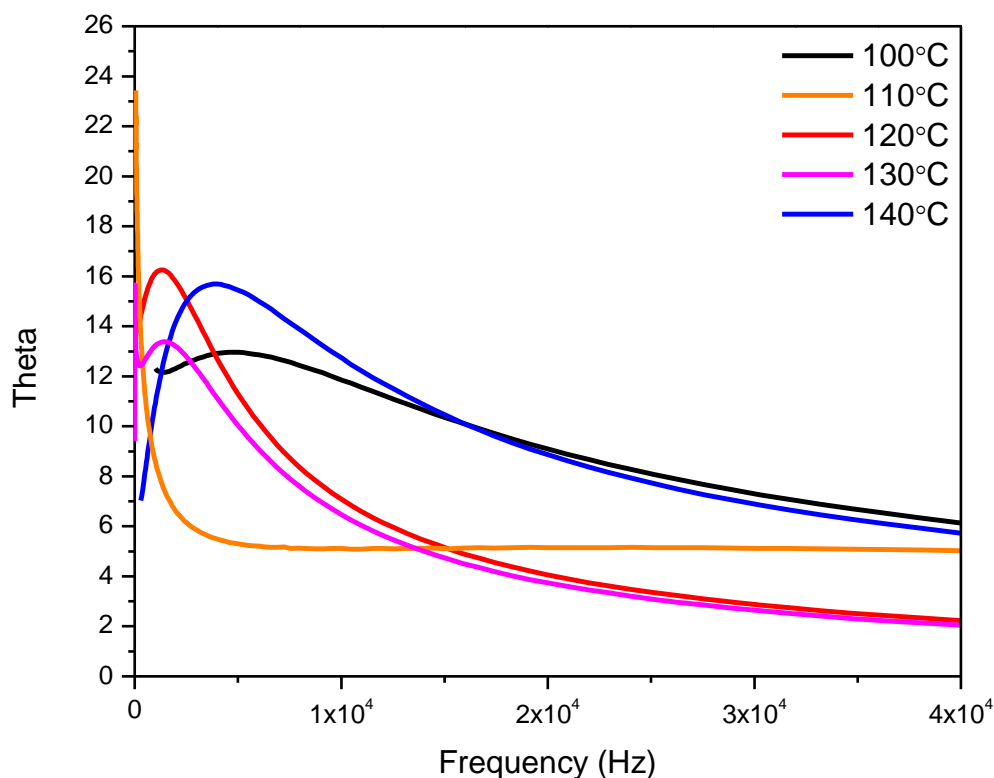


**Figure 7.** Bode plots with various annealing temperatures of gold doped RGO

Table 2 illustrates the photovoltaic and EIS parameters with various annealing temperatures of gold doped RGO counter electrode. According to the table, it was found that the DSSC utilizing the counter electrode prepared at  $120^\circ\text{C}$  performs the highest  $\eta$ . This is due to this device possesses the longest carrier lifetime. The  $\eta$  is affected by the properties of the device components such as morphology, optical and electrical properties of  $\text{TiO}_2$  photoanode, optical properties of dye, conductivity of electrolyte and electrical property of counter electrode. There is quite significant change in  $V_{\text{oc}}$ . However, the annealing treatment on the counter electrode does not increase  $V_{\text{oc}}$ . This is because  $V_{\text{oc}}$  is only influenced by the energy level of the device components such as the fermi level of  $\text{TiO}_2$ , energy gap of dye and energy level of counter electrode.

Generally, from Table 1, the  $FF$  is low since the area of maximum power rectangles drawn from the  $J$ - $V$  curves is much smaller than that of the  $J$ - $V$  curves shown in Fig. 3. The highest  $\eta$

obtained in this work, 0.134% is much smaller compared with those reported in [13-15] that are 4.99, 6.81 and 7.80%, respectively. This might be caused the internal resistance of the DSSC fabricated in this work is much higher than those reported in [13-15]. However, it is higher than that of the device utilizing pure rGO counter electrode reported in [11] which was 0.09%. The highest efficiency of 0.134% is slightly lower than that of the device utilizing platinum counter electrode, yielding the efficiency of 0.44% [18]. We did not study the performance stability of the DSSC utilizing this gold doped rGO. However, the device can last for one day upon the filling of the electrolyte containing iodide/triiodide redox couple.

**Table 2.** Photovoltaic parameters, EIS data and carrier lifetime with annealing temperatures of gold doped RGO

Temperature (°C)	$J_{sc}$ (mAcm <sup>-2</sup> )	$\eta$ (%)	(FF)	$V_{oc}$ (V)	$R_b$ ( $\Omega$ )	$R_{ct}$ ( $\Omega$ )	$\tau$ (s)
100	0.349	0.068	0.340	0.572	73	506	0.000219
110	0.308	0.051	0.345	0.476	27	400	-
120	0.510	0.134	0.340	0.568	96	516	0.000797
130	0.716	0.072	0.206	0.490	62	475	0.000725
140	0.773	0.100	0.234	0.553	100	194	0.000263

#### 4. CONCLUSIONS

Gold doped reduced graphene oxide (rGO) films were successfully prepared on ITO substrate and applied in DSSC as counter electrode. The optical transmittance of the samples changes with annealing temperature for which the 140 °C sample possesses the highest transmittance. The annealing treatment on the electrode has changed the performance of the DSSC utilizing gold doped rGO counter electrode. The resistance and carrier lifetime varies with annealing temperature. The DSSC utilizing the counter electrode annealed at 120 °C demonstrates the highest  $\eta$  due to the longest  $\tau$ .

#### ACKNOWLEDGMENTS

This work was supported by Universiti Kebangsaan Malaysia (UKM) under research grant DLP 2015-003 and GUP-2016-013.

#### References

1. Z. Huang, X. Liu, K. Li, D. Li, Y. Luo, Hong Li, W. Song, L. Chen and Q. Meng, *Electrochem. Commun.* 9 (2007) 596-598.
2. J.G. Nam, Y.J. Park, B.S. Kim and J.S. Lee, *Scripta Materialia* 62 (2010) 148-150.
3. H. Zhu, H. Zeng, V. Subramanian, C. Masarapu, K-H.Hung and B. Wei, *Nanotechnology* 19

- (2008) 465204 (5 pp).
4. J. D. Roy-Mayhew, D.J. Bozym, C. Punckt and I.A. Aksay, *ACS Nano* 4 (2010) 6203-6211.
  5. D.W. Zhang, X.D. Li, H.B. Li, S. Chen, Z. Sun, X.J. Yin and S.M. Huang, *Carbon* 49 (2011) 5382-5388.
  6. H. Wang, K. Sun, F. Tao, D. J. Stacchiola and Y.H. Hu, *Angew. Chem. Int. Ed.* 52 (2013), 9210-9214.
  7. L. Kavan, *Top Curr. Chem.* 348 (2014) 53-94.
  8. L. Kavan, J.-H. Yum and M. Grätzel, *Electrochim. Acta* 128 (2014) 349-359.
  9. M. Janani, P. Srikrishnarka, S.V. Nair and A.S. Nair, *J.Mater.Chem A* 3, (2015) 17914-17938.
  10. L. Kavan, P. Liska, S.M. Zakeeruddin and M. Grätzel *Electrochim. Acta* 195 (2016) 34-42.
  11. M.Y.A. Rahman, A.S. Sulaiman, A.A. Umar and M.M. Salleh, *J. Mater. Sci.: Mater. Electron.* 28 (2017) 1674-1678.
  12. L.T. Soo, K.S. Loh, A.B. Mohamad, W.R.W. Daud and W.Y. Wong, *J. Power Sources* 324 (2016) 412-420.
  13. Y. Xue, J. Liu, H. Chen, R. Wang, D. Li, J. Qu and L. Dai, *Angew. Chem. Int. Ed.* 51 (2012) 12124-12127.
  14. M.J. Ju,,J.C. Kim,, H.-J. Choi, ,I.T. Choi, S.G. Kim, K. Lim, J. Ko, J.-J. Lee, I.-Y. Jeon, J.-B. Baek and H. K. Kim, *ACS Nano* 6 (2013) 5243-5250.
  15. Z. Wang, P. Li, Y. Chen, J. He, J. Liu, W. Zhang and Y. Li, *J. Power Sources* 263 (2014) 246-251.
  16. M.Y.A. Rahman, M.M. Salleh, I.A. Talib and M. Yahaya, *Curr. Appl. Phys.* 5 (2005) 599-602.
  17. H. Choi, H. Kim, S. Hwang, W. Choi and M. Jeon, *Sol. Energy Mater. Sol. Cells* 95 (2011) 323-325.
  18. A.S. Sulaiman, M.Y.A. Rahman, A.A. Umar and M.M. Salleh, *Russian J. Electrochem.* 54 (2018) 56-61.

© 2018 The Authors. Published by ESG ([www.electrochemsci.org](http://www.electrochemsci.org)). This article is an open access article distributed under the terms and conditions of the Creative Commons Attribution license (<http://creativecommons.org/licenses/by/4.0/>).